

UNCLASSIFIED

Defense Technical Information Center
Compilation Part Notice

ADP012592

TITLE: InAsN Grown by Plasma-Assisted Gas Source MBE

DISTRIBUTION: Approved for public release, distribution unlimited

This paper is part of the following report:

TITLE: Progress in Semiconductor Materials for Optoelectronic Applications Symposium held in Boston, Massachusetts on November 26-29, 2001.

To order the complete compilation report, use: ADA405047

The component part is provided here to allow users access to individually authored sections of proceedings, annals, symposia, etc. However, the component should be considered within the context of the overall compilation report and not as a stand-alone technical report.

The following component part numbers comprise the compilation report:

ADP012585 thru ADP012685

UNCLASSIFIED

InAsN Grown by Plasma-Assisted Gas Source MBE

Ding-Kang Shih, Hao-Hsiung Lin, and Tso-Yu Chu, National Taiwan University, Dept. of Electrical Engineering, Taipei, Taiwan, R.O.C.

T. R. Yang, National Taiwan Normal University, Dept. of Physics, Taipei, Taiwan, R.O.C.

ABSTRACT

We report the structural, electrical and optical properties of bulk InAsN alloy with various nitrogen contents deposited on (100) InP substrates by using plasma-assisted gas source molecular beam epitaxy. It is found that the fundamental absorption edge of InAsN, as compared to that of InAs, shifts to higher energy due to Burstein-Moss effect. A dramatic increase of the electron effective mass in a nitrogen-containing III-V alloy is also observed from infrared reflectivity and Hall measurement on these degenerate InAsN samples. The sizeable increase on electron effective mass is consistent with the theoretical predictions based on band-anticrossing model.

INTRODUCTION

Group III-V-nitride alloys have a very large band-gap bowing due to the large valence electron energy of the nitrogen atom when compared to other group V atoms [1]. Over the last few years, there have been numerous attempts to explain the large band gap reductions properties of the III-V-N alloys. It has been demonstrated recently that a band anticrossing (BAC) model in which localized N states interact with the extended states of the conduction band can explain the unusual properties of the III-V-N alloys [2].

The huge bowing effect on the band gap energy makes InAsN alloy a promising material for infrared applications. However, only very limited efforts were put on this materials. In this report, we have investigated a series of unintentionally doped InAsN bulk layers with various N contents grown on InP substrates by using gas source molecular beam epitaxy (GSMBE). We found that these samples are with high residual carrier concentration, which increases as N composition increases. Furthermore, the fundamental absorption edge of InAsN, as compared to that of InAs, shifts to higher energy due to the Burstein-Moss (BM) effect [3]. To deduce the 'real' band gap energy of our InAsN samples, the energy shift due to BM effect and the band gap narrowing (BGN) effect are considered by using a self-consistent approach based on the BAC model. After the correction, the 'real' band gap energy of InAsN samples decreases as N increases, and follows the bowing effect normally. In addition, we found a dramatic increase of the electron effective mass in these InAsN alloys, which is consistent with the theoretical predictions based on BAC model.

EXPERIMENTAL DETAILS

The InAsN epitaxial layers were grown on semi-insulating InP substrates using GSMBE with RF plasma source as the nitrogen source. Layers were grown at 460°C at a growth rate of 1.5 $\mu\text{m/hr}$. The ranges of RF power and nitrogen flow rate were from 300W to 480W and from 0.5 to 1.9 sccm, respectively. Detailed growth conditions has been described elsewhere [4]. The thickness of InAsN epitaxial layer was 2 μm and the nitrogen composition of the InAsN sample was determined from the double crystal X-ray diffractometer (DXRD) spectra fittings by using a

commercial dynamic simulator, RADS. The electrical and optical properties of the samples were investigated by using a home-made Hall effect system and a Bruker IFS 120 HR Fourier transform infrared (FTIR) spectrometer, respectively.

DISCUSSION

Fig.1 shows the DXRD rocking curves of InAs and InAsN samples. As plasma power increased, the diffraction peak of the InAsN, as compared with that of InAs sample, shifts closer to the InP substrate peak. It represents that N was indeed incorporated into InAs. The results from RADS fitting were also listed in the Fig.1. Although N was added into InAs successfully, its incorporation also degrades the DXRD linewidths as compared to the referential InAs. Table I shows the Hall results of the samples at room temperature. All the undoped samples exhibited n-type conduction. It was found that the more the N composition, the higher the carrier concentration. The possible origin of the high carrier concentration in N-containing sample is not quite clear at the moment. However, because of the large InAs crystal lattice constant and the small N atom size, nitrogen interstitial defects could be a possible candidate. Furthermore, since the band gap is very narrow, the defect levels in these materials could be 'effective shallow' and thus could be ionized to result in high residual carrier concentration. As compared with other samples, sample C1078 has the largest residual free carrier concentration and an extraordinary low mobility. According to BAC model, the dispersion relation of the nonparabolic subbands become flatter as the nitrogen composition is increased. This indicates a large increase of the effective mass in the subbands. Furthermore, the higher residual free carrier concentration in sample C1078 may make the nonparabolic effect on the subband more significant, and therefore results in very low mobility. Fig. 2 shows the near band edge absorption spectra converted from FTIR transmission measurement at 300K. Two points are worthy of note from this figure. First, the energy of the absorption edge of InAsN samples is always higher than that of InAs. Second, when N composition is lower than 1.6%, higher N composition results in higher absorption edge. But, the trend reverses for InAsN with N composition larger than 1.6%. The phenomenon seems controversy to the theoretical prediction. To interpret the results, BM effect should be taken into account because of the high residual carrier concentration in these InAsN samples. Samples with lower N composition have smaller effective mass and thus more significant BM effects. The two high N content samples, however, have larger effective mass and thus their BM effects are less significant. In these two samples, C1078 (2.8%) and C1077 (1.6%), the bowing effect on band gap may have overcome the BM effect, and results in red-shifted absorption edge, though the carrier concentration of the former is five times higher than that of the latter.

To deduce the 'real' band gap energy of our InAsN samples, the energy shift due to BM effect and the BGN effect which is always accompanied by the BM effect are considered by using a self-consistent approach based on the BAC model. As the BAC model described, the interaction of the N states with the extended states of the semiconductor matrix transforms them into two nonparabolic subbands E_- and E_+ given by

$$E_{\pm}(k) = \frac{1}{2} \{ [E_M(k) + E_N] \pm \sqrt{[E_M(k) - E_N]^2 + 4V_{NM}^2} \}, \quad (1)$$

where E_N is the energy of the N state, $E_M(k)$ is the dispersion relation for the conduction band of the host crystal, and V_{NM} is the matrix element coupling those two types of states. All the energies are measured relative to the top of the valence band. The downward shift of the lower subband E_- can account well for the reduction of the fundamental band gap observed in these III-V-N alloys.

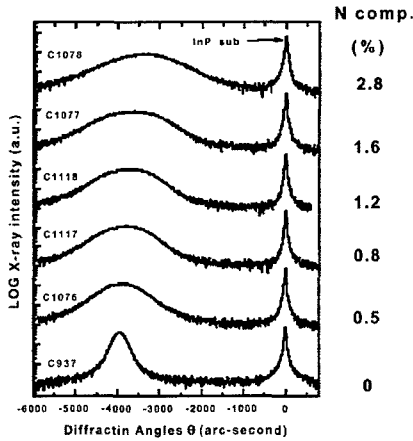


Figure 1. DXRD spectra of a series $\text{InAs}_{1-x}\text{N}_x$ bulk samples with x from 0 to 0.028.

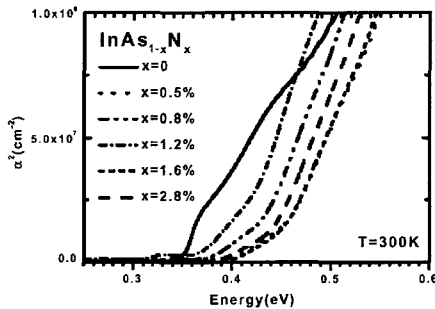


Figure 2. Plots of the square of the absorption coefficient (α^2) against the photon energy deduced from 300K IR transmission spectra recorded on a series of $\text{InAs}_{1-x}\text{N}_x$ bulk samples with x from 0 to 0.028

It is evident from Eq. (1) that the initial rate of the N-induced band gap reduction depends on the coupling parameter V_{NM} and on the energy difference $E_M - E_N$. Therefore the dependence of E_N , E_M , and V_{NM} on the nitrogen content of the InAsN bulk layer should be duly taken into account. Due to its localized nature [5], the energy E_N of the N level in InAsN case can be estimated 1.48 eV from the valence band offset, ΔE_V (GaAs/InAs) = 0.17 eV [6] and $E_N = 1.65$ eV in GaAs. Concerning the dispersion relation $E_M(k)$ for the conduction band of InAs , we adopted the calculation results of Ref. 7, which is based on triple-band effective-mass approximation, and $E_M(0) = 0.35$ eV at 300K. For V_{NM} , it has been shown previously that the square of the matrix elements is proportional to the concentration of nitrogen atoms, i. e., $V_{NM} = C_{NM}x^{1/2}$, where C_{NM} is a constant dependent on the semiconductor matrix and is treated as a fitting parameter in this study.

Table I. Nitrogen composition, carrier concentration, plasma frequency, experimental, and theoretical calculated electron effective mass of the studied samples.

Sample No.	N (%)	residual	Mobility (cm ² /V sec)	α_{λ} (cm ⁻¹)	m* (m ₀) <i>exp.</i>	m* (m ₀) <i>cal.</i>
		carrier conc. n _D (cm ⁻³)				
C937	0	2.64×10 ¹⁶	7660	-	-	0.024 [10]
C1076	0.5	1.91×10 ¹⁷	1740	471	0.063	0.044
C1077	1.6	3.24×10 ¹⁸	1280	590	0.068	0.052
C1078	2.8	1.69×10 ¹⁹	38.1	617	0.326	0.123
C1117	0.8	1.21×10 ¹⁸	2690	390	0.055	0.039
C1118	1.2	8.85×10 ¹⁷	3290	360	0.051	0.036
C1129	0.1	9.87×10 ¹⁷	3530	395	0.046	0.037
C1130	1.6	1.69×10 ¹⁸	2140	475	0.055	0.043
C1132	2.8	3.08×10 ¹⁸	1010	593	0.058	0.046

In our case, the absorption edge E_{abs} is

$$E_{\text{abs}} = E_{\text{c}} + E_{\text{BM}} - E_{\text{BGN}}, \quad (2)$$

where E_{BM} is the energy shift due to BM effect, E_{BGN} is the reduction energy due to BGN effect. To estimate E_{BM}, we solve the Fermi energy E_F in the conduction band from $n_D = \int f(E_{\text{c}})D(E_{\text{c}})dE_{\text{c}}$, where n_D is residual carrier concentration from the Hall measurements, f(E_c) is the Fermi-Dirac distribution, and D(E_c) is the density-of-states function in the lower subband conduction band, E_c. The BM shift in valence band is $E_V(k_F) = \frac{\hbar^2 k_F^2}{2m_h^*}$, where k_F is Fermi

wave number which is given by $k_F = (3\pi^2 n_D)^{1/3}$. m_h^{*} is the effective mass of the heavy-hole. We also assume that the perturbation induced by nitrogen on valence band can be omitted in InAsN. The absorption from the light-hole band is neglected because of its very low density of state. In addition, the band-gap narrowing due to band tails is not considered either. Now, we have the band-gap widening E_{BM} for carrier concentration n_D as E_{BM} = E_F + E_V(k_F). Concerning the BGN due to the residual carrier, the shrinkage in energy is proportional to the carrier concentration and an empirical relation [8] can be represented by $E_{\text{BGN}} = \alpha_{\text{InAsN}} n_D^{1/2}$, where α_{InAsN} is BGN coefficient.

With a given V_{NM}, the lower subband E(k) can be calculated using Eq. (1). We treat the parameter V_{NM} as a fitting parameter. Once E(k) is determined, we can further calculate the density of state D(E_c) and solve E_F using $n_D = \int f(E_{\text{c}})D(E_{\text{c}})dE_{\text{c}}$ with measured n_D. E_{BM} is thus found by using $E_V(k_F) = \frac{\hbar^2 k_F^2}{2m_h^*}$ and E_{BM} = E_F + E_V(k_F). With the calculated E(k), we may also find

the conduction band effective mass, $m_{\text{InAsN}}^* = \frac{1}{\hbar^2} \frac{d^2 E_{\text{c}}}{dk^2}$, where ħ is Planck's constant. The BGN coefficient α_{InAsN} can also be found as following [9] $\alpha_{\text{InAsN}} = [(\epsilon_{\text{InAsN}}/\epsilon_{\text{InAs}})(m_{\text{InAs}}^*/m_{\text{InAsN}}^*)] \alpha_{\text{InAs}}$, where ε_{InAs(N)} is the static dielectric constant of InAs(N), and we suggest that ε_{InAsN} = ε_{InAs} since the nitrogen composition is small in the present alloy. For InAs, m_{InAs}^{*} = 0.024m₀, where m₀ is the electron rest mass, and ε_{InAs} = 15.15 [10]. Based on the three effects proposed in Ref.11, the estimated band-gap renormalization energy of InAs increases from ~40 meV to ~100 meV when carrier concentration increases from n~4×10¹⁸cm⁻³ to ~5×10¹⁹cm⁻³. By using the empirical

formula $E_{BGN} = \alpha_{InAs} n_D^{1/3}$, the BGN coefficient α_{InAs} should be $\sim 2.67 \times 10^{-8}$ meV cm. This value is adopted in this study to estimate α_{InAsN} for the determination of the energy shift caused by BGN effect. Once the E_c , E_{BM} , and E_{BGN} were determined, E_{abs} was found from Eq. (2). If the difference between the calculated E_{abs} and the experimental result was larger than 10^{-4} eV, a new V_{NM} was chosen by using the bisection method to calculate a new E_{abs} .

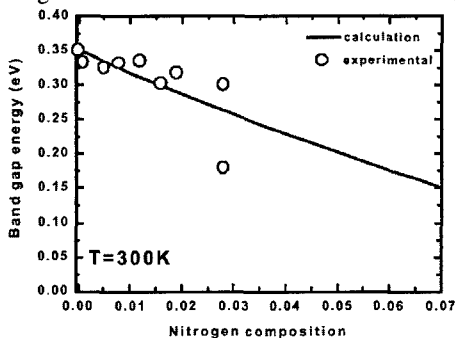


Figure 3. Composition dependence of the band gap of InAsN. The solid circles are experimental data and the solid line is calculated with the BAC model.

Table II gives the values of the E_c , E_{BM} , E_{BGN} , E_F and V_{NM} obtained from the above calculation, along with the residual carrier concentration N_D and absorption edge E_{abs} from the experiments. By fitting of $V_{NM} = C_{NM} x^{1/2}$ to the plot of V_{NM} versus the square root of nitrogen composition ($x^{1/2}$), the best fitted C_{NM} , the coupling parameter, in InAs, is 1.92eV.

Deducting the effect of E_{BM} and E_{BGN} on the band gap from the absorption peak edge gives the corrected band gap energy E_c of each InAsN sample. Fig. 3 shows the composition dependence of the corrected band gap energy of InAsN. It is clear that the bowing effect reappears in these samples. The solid line in this figure represents band gaps calculated based on BAC model carried out in this study. As can be seen, the experimental results are close to the theoretical curve calculated based on BAC model. The estimated transition energy shrinkage coefficient of our bulk InAsN is -14 meV/at %.

Table II. A summary of the computed and experimental energy involved in the self-consistent approach as described in the text. All energies are in eV.

Sample No.	N (%)	E_{abs}	E_F	$E_V (k_F)$	E_{BM}	E_{BGN}	E_c
C1076	0.5	0.439	0.134	0.013	0.147	0.032	0.324
C1077	1.6	0.439	0.157	0.019	0.176	0.038	0.301
C1078	2.8	0.434	0.255	0.061	0.316	0.061	0.179
C1117	0.8	0.419	0.106	0.01	0.116	0.028	0.331
C1118	1.2	0.405	0.089	0.007	0.096	0.025	0.334
C1129	0.1	0.409	0.094	0.008	0.102	0.026	0.333
C1130	0.5	0.415	0.117	0.012	0.129	0.021	0.317
C1132	2.8	0.423	0.142	0.017	0.159	0.036	0.300

To verify the effective mass increment predicted by BAC models, we performed measurements of the infrared reflectivity and Hall effect from which the plasma frequency ω_p and Hall electron concentration n_D in these InAsN samples were determined. The plasma frequency and the calculated electron effective mass of InAsN samples are summarized in Table I. As can be seen, a very large increase of the effective mass is found in samples with higher N composition, which it is in good qualitative agreement with the predictions of the BAC model. The electron effective mass of the C1078 is extraordinary larger than other samples. This result supports the arguments we use to interpret the extraordinary low mobility for the same sample in previous Hall results.

CONCLUSION

InAsN alloys with various N compositions were successfully grown on InP substrate by using plasma-assisted GSMBE. When N composition increases, InAsN film has broader FWHM in DXRD spectrum and higher residual carrier concentration. Dramatic increase on the electron effective mass and decrease on the carrier mobility due to the N incorporation in InAsN alloy were observed. The absorption edge of InAsN alloy, as compared to that of InAs, shows blue-shift energy. After considering the energy shift due to residual carrier concentration from the absorption peak edge based on the band anticrossing theory, the bowing effect reappears in these InAsN samples.

Acknowledgement

This work was supported by the National Science Council and the Ministry of Education of the Republic of China under Contract No. NSC 89-2215-E-002 -034 and 89-N-FA01-2-4-3, in respectively.

REFERENCE

1. M. Kondow, K. Uomi, T. Kitatani, S. Watahiki, and Y. Yazawa, *J. Crystal Growth* **164**, 175 (1996).
2. W. Shan, W. Walukiewicz, J. W. Ager III, E. E. Haller, J. F. Geisz, D. J. Friedman, J. M. Olson, and S. R. Kurtz, *Phys. Rev. Lett.* **82**, 1221 (1999).
3. E. Burstein, *Phys. Rev.* **93**, 632 (1954).
4. D. K. Shih, H. H. Lin, L. W. Song, T. Y. Chu, and T. R. Yang, *Proceeding of 13th Indium Phosphide and Related Materials*, Nara, Japan (2001), p.555.
5. H.P. Hjalmarson, P. Vogl, D. J. Wolford, and J. D. Dow, *Phys. Rev. Lett.* **44**, 810 (1980).
6. Y. C. Ruan and W. Y. Ching, *J. Appl. Phys.* **262**, 2885 (1987).
7. J. Stiens and R. Vounckx, *J. Appl. Phys.* **76**, 3526 (1994).
8. X. Zhang, S. J.Chua, W. Liu, and K. B. Chong, *Appl. Phys. Lett.* **72**, 1890 (1998).
9. D. C. Reynolds, D. C. Look, and B. Jogai, *J. Appl. Phys.* **88**, 5760 (2000).
10. V. Swaminathan and A. T. Macrander, *Materials Aspects of GaAs and InP Based Structures* (Prentice-Hall, New Jersey, 1991), p.21.
11. W. Dobbelaere, J. De Boeck, P. Van Mieghem, R. Mertens, and G. Borghs, *J. Appl. Phys.* **69**, 2536 (1991).